STATE OF THE CLIMATE IN 2008

T. C. Peterson and M. O. Baringer, Eds.

Associate Eds.: H. J. Diamond, R. L. Fogt, J. M. Levy, J. Richter-Menge, P. W. Thorne, L. A. Vincent, and A. B. Watkins

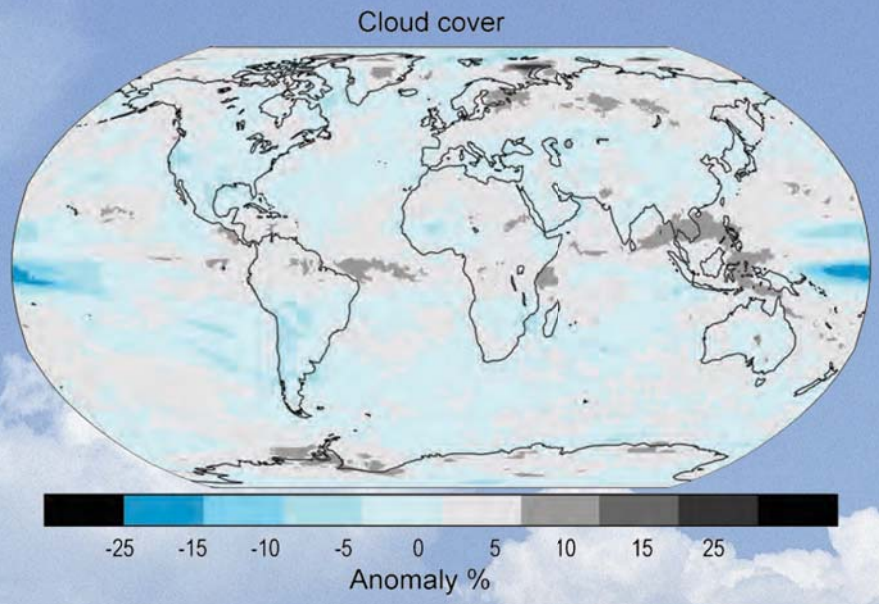

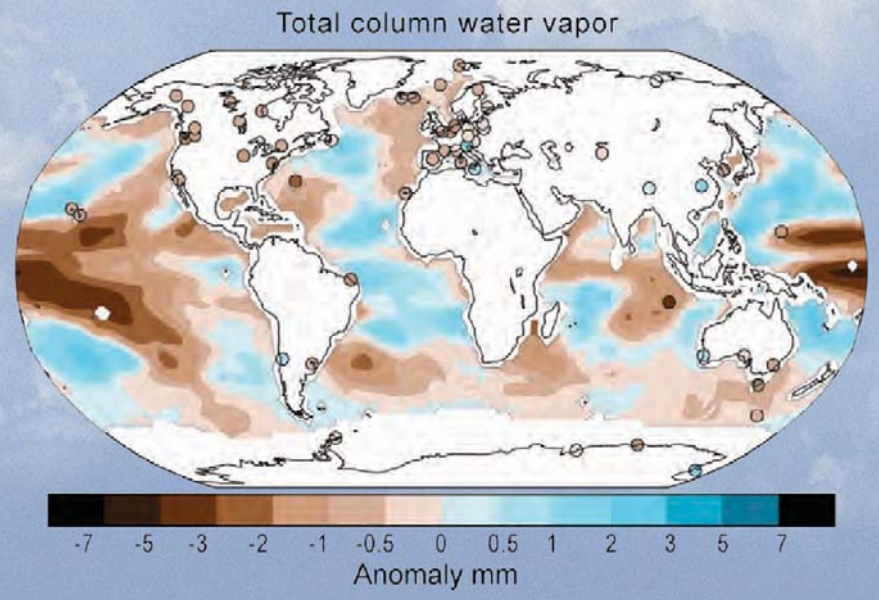

Special Supplement to the *Bulletin of the American Meteorological Society*
Vol. 90, No. 8, August 2009

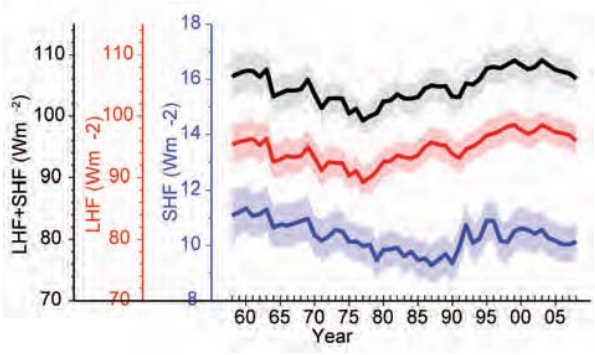

Fig. 3.9. Year-to-year variations of global-averaged annual mean latent plus sensible heat flux (blue line), latent heat flux (red line), and sensible heat flux (black line). The shaded areas indicate the upper and lower limits at the 90% confidence level.

ruled by intricate feedbacks between the ocean and the atmosphere. The oceans modulate large-scale climate variability and change, while short-term weather events could impose significant impact on ocean variability and thus impart an indelible signature on the long-term climate of the ocean circulation. It is worth noting that changes in air–sea heat fluxes also affect the hydrological cycle and hence ocean salinity, as the evaporation releases not only latent heat but also water vapor to the atmosphere. The structure of LHF + SHF anomalies, in particular the tripole shape in the North Atlantic Ocean, was in broad agreement with that of surface salinity anomalies (Fig. 3.13b). The freshening of the sea surface (i.e., negative surface salinity anomalies) over the Gulf Stream was in tune with the local weakened evaporation (i.e., negative LHF + SHF anomalies), while the increased surface salinity to the north and south coincided with enhanced evaporation forcing (positive LHF + SHF anomalies).

The basin-averaged LHF + SHF in 2008 was slightly down from 2007, continuing the broad downward trend that started in 1999 (Fig. 3.9). There seems to be a tendency toward reversing the upward trend that had dominated the decades of 1980s and 1990s.

e. *Tropical cyclone heat potential*—G. J. Goni and J. A. Knaff

Tropical cyclones occur in seven regions in all ocean basins: tropical Atlantic, northeast Pacific, northwest Pacific, southwest Indian, north Indian, southeast Indian, and South Pacific. While SST plays a role in the genesis of TCs, the ocean heat content contained between the sea surface and the depth of the 26°C isotherm, also referred to as TCHP, has been shown to play a more important role in TC intensity changes (Shay et al. 2000), provided that atmospheric conditions are also favorable. The TCHP shows high spatial and temporal variability associated with oceanic mesoscale features. Sea surface height observations derived from satellite altimetry can be used to compute the TCHP (Goni et al. 1996; Shay et al. 2000). In general, the real-time forecast of TC intensity is highly dependent on track forecasts, and many of the errors introduced in the track forecast are translated into the intensity forecast. Clearly, areas with high values of TCHP may be important only when TCs travel over them.

To examine the interannual variability of TCHP with respect to tropical cyclones, TCHP anomalies are computed during the months of TC activity in each hemisphere: June through November in the Northern Hemisphere and November through April in the Southern Hemisphere. Anomalies are defined as departures from the mean TCHP calculated during the same months for the period 1993 to 2008. These anomalies show large variability within and among the tropical cyclone basins (Fig. 3.10).

The west Pacific basin exhibits the anomalies from the signature of the negative phase of the 2007 ENSO event (La Niña). The South Pacific basin showed mostly positive anomalies. The north Indian Basin exhibited positive values in the Bay of Bengal and in the eastern Arabian Sea and negative values in the

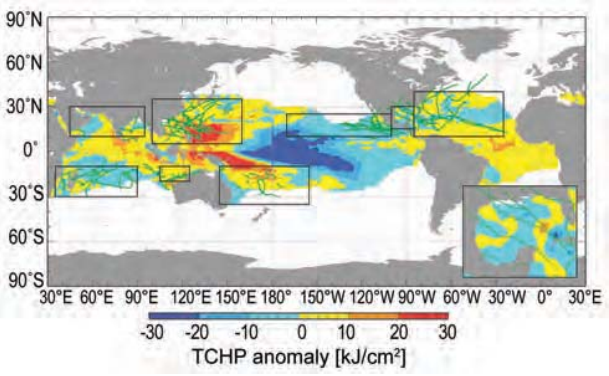

Fig. 3.10. Global anomalies of TCHP corresponding to 2008 computed as described in the text. The boxes indicate the seven regions where TCs occur: (left to right) southwest Indian, north Indian, west Pacific, southeast Indian, South Pacific, east Pacific, and North Atlantic (shown as Gulf of Mexico and tropical Atlantic separately). The black lines indicate the trajectories of all tropical cyclones Category 1 and above during Nov 2007 through Dec 2008 in the Southern Hemisphere and Jan through Dec 2008 in the Northern Hemisphere. The Gulf of Mexico conditions during Jun through Nov 2008 are shown in detail in the insert shown in the lower right corner.

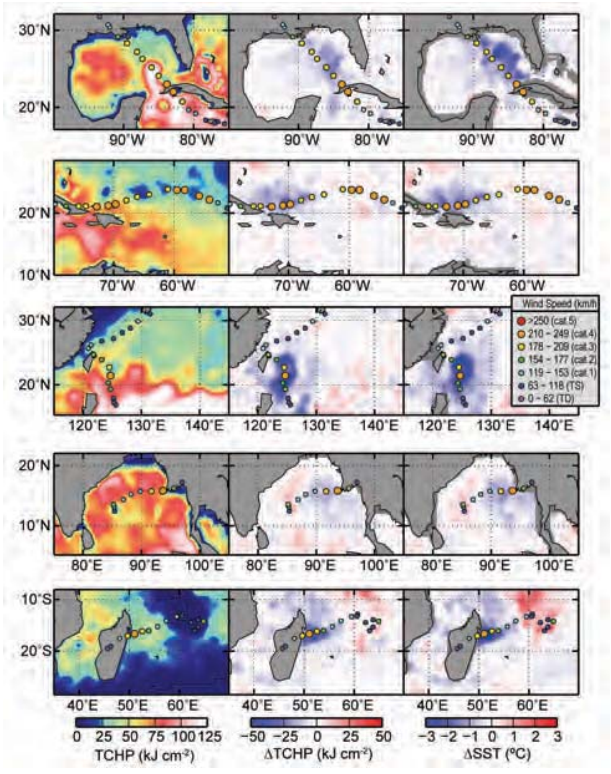

Fig. 3.11. (left) Tropical cyclone heat potential and surface cooling given by the difference between post- and prestorm values of (center) tropical cyclone heat potential and (right) sea surface temperature, for (from top to bottom) Hurricane Gustav, Hurricane Ike, Typhoon Sinlaku, Tropical Cyclone Nargis, and Tropical Cyclone Ivan.

western Arabian Sea. The Gulf of Mexico (insert) showed an alternation of regions with positive and negative values. The tropical Atlantic exhibited positive values to the north of 30°N and south of 15°N. The most evident changes that happened between 2008 and 2007 are the increase of values in the southern region of the western Pacific basin.

During 2008 several TCs were identified to have gained strength when traveling into regions of very high or higher values of TCHP. Some examples of these intensification events are shown in Fig. 3.11. The results presented here correspond to five intense (Categories 4 and 5) TCs, where the location of their intensification coincided with an increase of the values of TCHP along their tracks. Additionally, the cooling associated with the wake of the TCs, which can reach values of 30 kJ cm^{-2} in tropical cyclone heat potential and 3°C in sea surface temperature, is important because it influences the upper-ocean thermal structure on regional scales within weeks to months after the passage of the cyclones. These TCs were Gustav in the Gulf of Mexico, Ike in the Caribbean Sea, Sinlaku in the western Pacific, Nargis in the northern Indian, and Ivan in the southwest Indian region. A brief description of each of these storms is now presented.

In the Atlantic basin, Hurricanes Gustav and Ike are good examples of major hurricanes that interacted with TCHP features. Hurricane Gustav (25 August–2 September) reached its maximum estimated intensity of 125 kt prior to making landfall in Cuba on 30 August and at a time when its track was traversing some of the highest values of TCHP west of Jamaica. The storm's impact was felt throughout the northern Caribbean in Hispanola, Jamaica, the Cayman Islands, and Cuba. On the other hand, Hurricane Ike (1–14 September) experienced three separate peak intensities. The first and maximum peak intensity, 125 kt, was obtained in the central Atlantic, northwest of the Leeward Islands. In the next day or so, the storm weakened and moved southwest. The second peak shown in Fig. 3.11 occurred in a region of elevated TCHP. The third peak intensity occurred in the Gulf of Mexico before making landfall in Texas (not shown in Fig. 3.11). This storm resulted in major impacts throughout the northern Caribbean, making landfall twice in Cuba (110, 115 kt) and once in Texas (95 kt).

Typhoon Sinlaku (8–22 September), in the western North Pacific, obtained its maximum intensity (125 kt) following an encounter with a warm ocean eddy. Following its peak intensity, the storm weakened slightly as it turned toward Taiwan and moved over lower values of TCHP. Following this weakening, Sinlaku showed a slight intensification as it tracked to the northwest and moved over larger TCHP values. The storm eventually brushed the northeast coast of Taiwan on 13 September with an estimated intensity between 90 and 95 kt.

In the north Indian Ocean, Tropical Cyclone Nargis (27 April–3 May) made landfall in Myanmar on 2 May with an estimated intensity of 115 kt. The storm resulted in a devastating surge that killed an estimated 146,000 people. The storm intensified over the high TCHP waters of the Bay of Bengal. One aspect of the storm's forecast is that for the 48 h prior to landfall the storm was forecasted to have a more northward track than was observed, which not only allowed the storm to track over higher TCHP values but to make landfall in the low-lying Irrawaddy River delta. This storm occurred in early May and likely contributed to the negative anomalies in Fig. 3.10 in the northern part of the Bay of Bengal.

Tropical Cyclone Ivan (7–22 February) is a good example of a very strong and rather large Southern Hemisphere tropical cyclone, which reached its

maximum intensity of 115 kt just as it made landfall in Madagascar. Ivan also tracked across the warmest TCHP during the day or so prior to landfall on 17 February when intensification was occurring. Initial reports indicated that 26 deaths occurred and more than 300,000 persons were affected, particularly by the heavy general rainfall and subsequent floods in the north and east of the island of Madagascar.

Hurricane Gustav (2008) is now contrasted with Hurricane Katrina (2005) (Fig. 3.12). Both hurricanes made landfall in a region in the Gulf of Mexico. There are some similarities as they both traveled directly over the Loop Current. Katrina was energized by its passage over the Loop Current and continued to intensify as it moved from the Loop Current region into a region occupied by a warm ring shed by the Loop Current. The storm also became larger as it went through an eyewall replacement cycle (Maclay et al. 2009). Gustav, in contrast, tried to reorganize over the Loop Current region following a landfall in western Cuba, but instead of moving over a warm eddy as Katrina did, Gustav moved into a region of relatively low TCHP and did not reintensify despite being in favorable environmental conditions (200–850-hPa vertical wind shear <15 kt and SST >29°C). As a likely consequence, Gustav did not become nearly as large or as intense as Katrina. And while both storms weakened as they approached the Louisiana coast, Katrina with its larger and more intense wind field and landfall in a more populated area produced more property damage. The difference in the intensity of these two hurricanes translates into a difference in sea surface cooling. Maximum cooling by Katrina was approximately 30 kJ cm^{-2} in tropical cyclone heat potential and 4°C in sea surface temperature, almost double that observed for Hurricane Gustav.

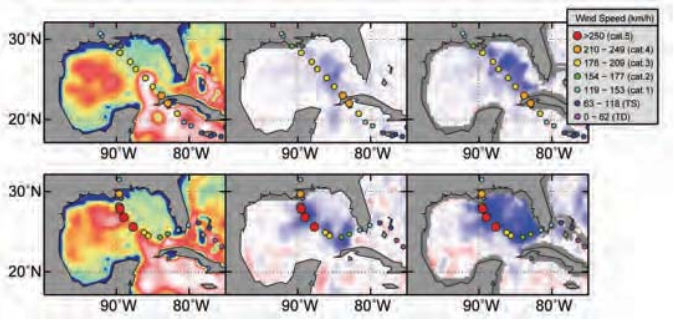

Fig. 3.12. (left) Tropical cyclone heat potential and surface cooling given by the difference between post- and prestorm values of (center) tropical cyclone heat potential and (right) sea surface temperature, for Hurricanes (bottom) Katrina in 2005 and (top) Gustav in 2008. The scales are the same as in Fig. 3.11.

f. Sea surface salinity—G. C. Johnson and J. M. Lyman

Ocean storage and transport of freshwater are intrinsic to aspects of global climate including the water cycle (e.g., Wijffels et al. 1992), El Niño (e.g., Maes et al. 2006), and anthropogenic climate change (e.g., Held and Soden 2006). In the past, in situ ocean salinity data have been too sparse and their reporting too delayed for an annual global perspective of ocean freshwater and its complement, salinity. However, over the past few years, the now mature Argo array of profiling floats, which measures temperature and salinity year-round in the upper 2 km of the ice-free global ocean (Roemmich et al. 2004), has remedied this situation. In addition, remote sensing of SSS by satellite is planned for 2010 (http://aquarius.gsfc.nasa.gov/).

The near-global Argo data are analyzed here to determine an annual average SSS anomaly for 2008 relative to a climatology and to describe how annual SSS anomalies have changed in 2008 relative to 2007. In this work the shallowest near-surface (<25 m) salinity data flagged as good from each available Argo profile for 2007 and 2008 were subjected to a statistical check to discard outliers. After this statistical check, the remaining data were then cast as differences from a climatological mean surface salinity field from the *WOA* based on historical data reported through 2001 (*WOA* 2001; Boyer et al. 2001). The resulting anomalies were then mapped (Bretherton et al. 1976) assuming a Gaussian covariance function with 6° latitude and longitude decorrelation length scales and a noise-to-signal variance ratio of 2.2. While some delayed-mode scientific controlled (final) Argo data are available for the 2007–08 time period, many real-time (preliminary) Argo data were used in both years. The real-time estimates of SSS made here could change after all the data have been subjected to careful scientific quality control.

Climatological SSS patterns are correlated with surface freshwater flux: the sum of evaporation, precipitation, and river runoff (e.g., Bäranger et al. 1999) where advection processes are not dominant. In each ocean basin, subtropical salinity maxima centered between roughly 20° and 25° in latitude are signatures of the predominance of evaporation over precipitation. Conversely, in most regions where climatological surface salinities are relatively fresh, such as the high latitudes and the ITCZs, precipitation generally dominates over evaporation.

The 2008 anomalies from *WOA* 2001 (Fig. 3.13a) reveal some large-scale patterns